Single-Pixel Scanning Near-Field Imaging With Subwavelength Resolution Using Sharp Focusing Mikaelian Lens

Wenyi Shao and Qiang Chen, *Senior Member, IEEE*

***Abstract*— Obtaining sharp focusing with high resolution is of significant importance to microwave and millimeter-wave imaging and sensing. Here, we propose an all-dielectric surface focusing Mikaelian lens operating at the *X*- and *Ka*-band, respectively, with the high-resolution focusing of theoretical full-width half-maximum (FWHM) around 0.45λ for the single-pixel scanning microwave and millimeter-wave imaging. Benefitting from easily accessible 3-D printing, the designed lens prototype with perforation and infill structure can be fabricated at a very low cost. Moreover, numerical simulations and the spatial resolution imaging experimental results demonstrate that the proposed lens prototype exhibits excellent imaging performance with a subwavelength resolution of ∼0.5λ while maintaining broadband behavior, revealing great potential for high-resolution microwave and millimeter-wave imaging applications.**

***Index Terms*— Mikaelian lens, millimeter-wave imaging, near-field imaging, subwavelength-focused.**

I. Introduction

HIGH-RESOLUTION quasi-optical system for microwave and millimeter-wave imaging has received significant interest in recent years for a wide range of applications, including security imaging [1], [2], [3], nondestructive detection [4], and biomedical examinations [5], [6], due to the penetrating capabilities of microwave and millimeter-wave with nonionizing radiations. There are three common parameters for evaluating imaging systems [7]: spatial resolution, contrast, and depth of view. Among these parameters, spatial resolution is the most crucial parameter that defines imaging quality. Unfortunately, microwave and millimeter wave have a long wavelength compared with those of visible light, which inherently limit the resolution of imaging. In order to obtain the diffraction-limited images with high spatial resolution, imaging systems must require a large physical aperture of lens that make the overall system more bulky, complex, and high cost.

As one of the most critical devices in quasi-optical imaging systems, lens is particularly expected to achieve high-resolution focusing with large numerical aperture (NA) and broadband bandwidth. There are several well-known types of lenses, such as solid immersion lens [8], superoscillation lens [9], and meta-lens [10]. Although high-resolution focusing can be achieved by these lens types, the problem of small NA and narrow bandwidth still exists. Most importantly, the related research of these lenses mainly focuses on optical imaging applications. Considering the requirements of manufacturing materials and fabrication process in the microwave and millimeter-wave engineering, it is still a great challenge to apply these optical lens concepts in the microwave and millimeter-wave imaging system. Recently, a self-focusing hyperbolic secant (H-S) gradient index (GRIN) lens (also known as the Mikaelian lens) that can focus wave at the central axis of the lens periodically as shown in Fig. 1(a) has received increasing attention not only in the field of optics but also in microwave engineering. Once the oscillation period (P) called pitch is determined, various interesting phenomena, such as converging and point-to-point imaging, can be observed by choosing the appropriate length of lens. Moreover, it is free from spherical aberrations. The off-center rays have the same focusing behavior as paraxial rays, which enables to focus rays to the smallest possible spot on a subwavelength scale. For the case of $P = 0.5$, if a point source is placed at the center point of lens front surface, the rays intersect perfectly at a focal point on the rear surface of lens, as shown in Fig. 1(c). This feature mapping objects points to image points offers a great potential for imaging applications.

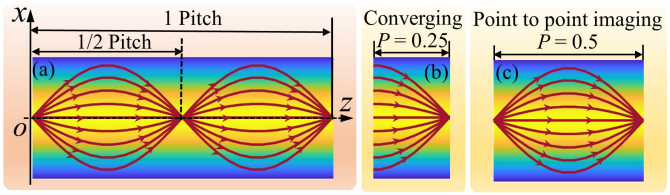

Fig. 1. (a) Mikaelian lens with unique propagation characteristics of self-focusing. Special cases for various interesting phenomena such as (b) converging and (c) point-to-point imaging with different pitches.

In [11], a planar binary H-S lens to generate a near-surface focal spot with full-width at half-maximum (FWHM) of 0.102λ was reported. Then, a nanoslit structure was utilized in a silicon-based planar H-S micro-lens in [12], which further improves the resolution to 0.043λ. The tight focusing of second-order cylindrical vector beams by an H-S lens was investigated in [13]. The diffraction limit, in this case,

Manuscript received 21 July 2022; accepted 17 August 2022. *(Corresponding author: Wenyi Shao.)*

The authors are with the Department of Communications Engineering, Tohoku University, Sendai 980-8579, Japan (e-mail: wenyi.shao.s1@alumni.tohoku.ac.jp; qiang.chen.a5@tohoku.ac.jp).

This article has supplementary material provided by the authors and color versions of one or more figures available at https://doi.org/10.1109/TMTT.2022.3205911.

Digital Object Identifier 10.1109/TMTT.2022.3205911

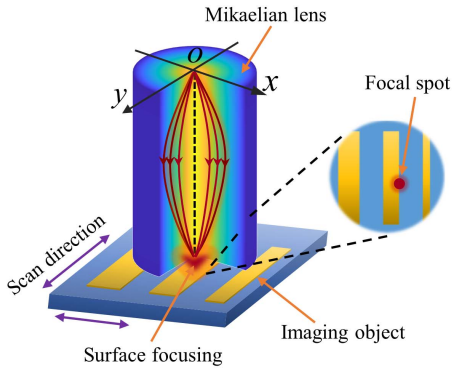

Fig. 2. Schematic of surface focusing Mikaelian lens ($P = 0.5$) for single-pixel scanning imaging application.

is FWHM $= 0.154\lambda$. Furthermore, the frequency response and polarization dependence photonic crystal Mikaelian lens in hexagonal and rectangular lattices was explored in [14] to evaluate the possibility of transverse focusing application in optical fiber. However, all these previous studies mainly focused on the focusing property for typical case ($P = 0.25$) of 2-D planar Mikaelian lens, which are only analyzed and validated by full-wave numerical simulation. There is not much information about how to put this lens concept into practice, not to mention the practical imaging application. However, in [15], [16], and [17], it was proven that an all-dielectric perforation structure can offer a potential technique for fabricating the Mikaelian lens in a microwave frequency range. Moreover, the possibility of subwavelength microwave imaging by using a 2-D planar Mikaelian lens ($P = 0.25$) with FWHM around 0.2λ as well as large NA of 2.04 at a frequency range of 7–14 GHz was indirectly demonstrated in [17].

However, despite all this, this unique characteristic of surface focusing provides a potential way to ensure a higher NA, which produces a more highly resolved image. The purpose of this article is to apply surface focusing Mikaelian lens with a compact structure, simple fabrication process, and cost-effectiveness into a single-pixel scanning microwave and millimeter-wave imaging application. In order to create a 2-D image, a designed Mikaelian lens equipped with a single receiving antenna needs to be moved linearly along the x- and the y-axis to scan across the surface of imaging object, as shown in Fig. 2. Due to a very small focal spot with the theoretical FWHM of 0.45λ at the rear surface of designed lens in this article, only a small area with the subwavelength spatial scale is illuminated during each movement period, which guarantees excellent imaging performance with high resolution.

Furthermore, the proposed lens prototype operating at the *X*- and *Ka*-band is all-dielectric, which can be fabricated by easily accessible 3-D printing techniques at a very low cost. By combining ray-tracing analysis and full-wave electromagnetic simulation, the surface focusing properties of subwavelength spot size for the designed lens are validated at the *X*- and *Ka*-band, revealing the advantage of broad bandwidth, Besides, its imaging performance at the *X*- and *Ka*-band is explored with the spatial resolution imaging experiment, which indicates that the spatial resolution of 0.5λ for designed lens prototype can be achieved in these two frequency bands.

The layout of this article is summarized as follows. Section II discusses the design theory, fabrication, and simulation verification of subwavelength surface focusing for the proposed Mikaelian lens operating at the *X*- and *Ka*-band. In Section III, the spatial resolution imaging experiment is carried out to verify the excellent imaging performance of designed lens. Conclusions are drawn in Section IV.

II. Surface Focusing of Mikaelian Lens

A. Realization of Mikaelian Lens for Microwave/Millimeter-Wave Imaging Using 3-D Printing Technique

The transverse refractive index profile of Mikaelian lens varies with the variable x, according to the following [18]:

$$n(x) = n_0 \sec h(2\pi Px/L) \tag{1}$$

where n_0 is the central refractive index along the z-axis, x is the coordinate in the transverse plane (xoz plane), P is the oscillation period (called pitch) of the rays inside lens, and L is the length of lens.

There are various manufacturing technologies such as foam pressing, PCB milling, and metamaterials with metallic resonant structures to fabricate GRIN lens. However, compared to 3-D printing, these manufacturing techniques need a complicated and expensive special fabrication process. Here, based on easily accessible 3-D printing, two fabrication processes using the internal perforation structure of various air-hole sizes [19] and different infill ratios of material [20] are utilized to achieve intended refractive index profile of Mikaelian lens for microwave and millimeter-wave imaging, respectively. Polylactic acid (PLA) plastic material is one of the most used 3-D printing materials, which has a relative dielectric constant $\varepsilon_m = 2.8$. The specific design procedure of two fabrication processes mentioned above is given as follows.

1) Perforation Structure for Microwave Imaging at X-Band: The pitch, diameter, and length of designed Mikaelian lens operating at the *X*-band are 0.5, 70 mm, and 133 mm, respectively. Fig. 3(a)–(d) shows the design steps of lens operating at 10 GHz. The 2-D continuous relative permittivity distribution of lens needs to be discretized first. Here, the unit-cell element is a cube with circular air hole, which has a size of 7×7 mm. After discretizing, the corresponding grid sizes are 19×10. The different sizes of air hole can be utilized to obtain the intended discrete effective permittivity (ε_{peff}), which can be calculated using the following expression [19]:

$$\varepsilon_{peff} = \frac{(a^2 - \pi b^2)\varepsilon_m + \pi b^2 \varepsilon_{\text{air}}}{a^2} \tag{2}$$

where a is the size of unit-cell element, b is the radius of circular air hole, and ε_{air} and ε_m are the air permittivity and the material permittivity, respectively.

In order to generate the cylindrical Mikaelian lens, the discrete 2-D air-hole structure needs to be rotated around the central axis, as shown in Fig. 3(d). In addition, the lens with perforation structure can be easily fabricated as a whole object by a one-stage process in fused deposition modeling (FDM) 3-D printer. In this process, additional processing is

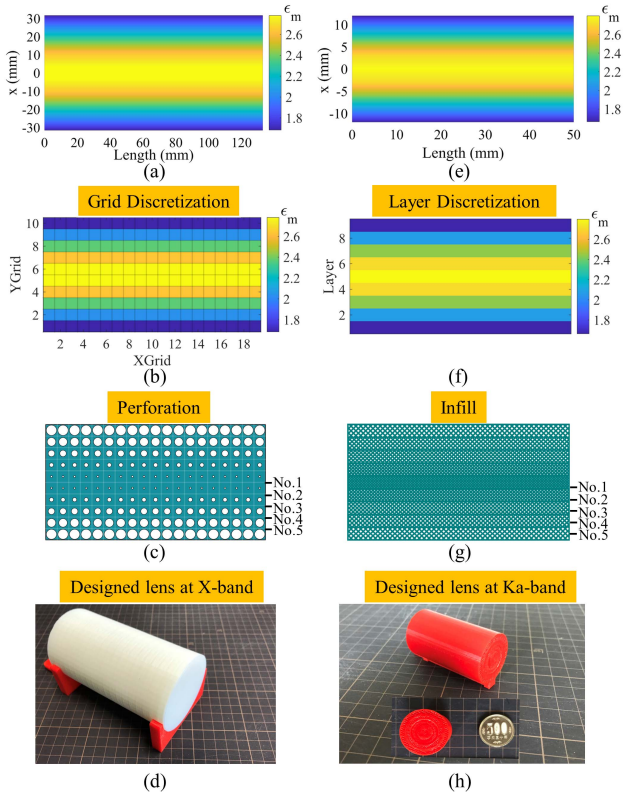

Fig. 3. (a)–(c) Design procedure of Mikaelian lens operating at the *X*-band with perforation structure. (d) Fabricated prototype of designed lens at the *X*-band. (e)–(g) Design procedure of Mikaelian lens operating at the *Ka*-band with different infill ratios. (h) Fabricated prototype of designed lens at the *Ka*-band.

not required. However, the warping phenomenon of FDM 3-D printing would cause hole shrinkage and deformation, which further affects the performance of the lens. The parametric studies have been carried out to evaluate the influence of manufacturing errors of lens on imaging resolution in Section II-C.

2) Infill Structure for Millimeter-Wave Imaging at Ka-Band: Considering the practical dimensional accuracy of the FDM 3-D printer, the air-hole structure cannot be fabricated in infinitely small size, which limits its imaging application in the high frequency. However, by controlling the infill ratio of PLA (PLA volume percentages), the functionality of the proposed lens concept can be easily expanded to higher frequency bands such as millimeter wave.

According to [20], the relationship between the effective permittivity ($\varepsilon_{i\text{eff}}$) and infill ratio ($v_{\text{ir}}$) is approximately linear, which can be determined by the following:

$$\varepsilon_{i\text{eff}} = 1 + v_{\text{ir}}(\varepsilon_m - 1) \tag{3}$$

where ε_m is the relative permittivity of the PLA at 100% infill.

Here, the pitch, diameter, and length of designed Mikaelian lens operating at the *Ka*-band are 0.5, 27 mm, and 50 mm, respectively. Unlike the abovementioned grid discretization, the 2-D continuous relative permittivity distribution of lens needs to be discretized into nine layers correspondingly. The different infill ratios of PLA are utilized to achieve the intended discrete permittivity distribution of each layer, as shown in Fig. 3(g).

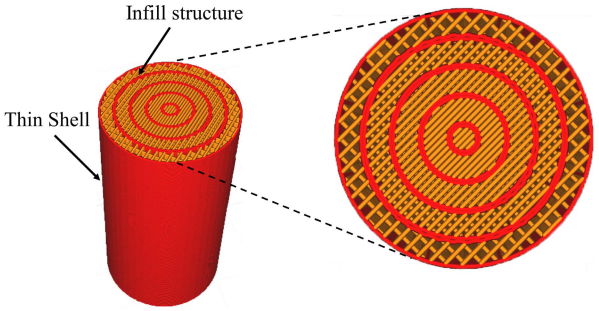

Fig. 4. Slicing model of the multilayer lens structure with different infill ratios of each layer generated by open-source Ultimaker Cura.

TABLE I
AIR-HOLE SIZES AND INFILL RATIOS WITH THE CORRESPONDING LAYER

X-band			Ka-band		
Layer (No.)	Air-hole diameter (mm)	ε_{peff}	Layer (No.)	Infill ratio (%)	ε_{ieff}
1	0.571	2.762	1	98.6	2.775
2	1.250	2.620	2	93.4	2.681
3	1.947	2.362	3	79.1	2.423
4	2.574	2.035	4	58.9	2.061
5	3.108	1.685	5	36.9	1.665

There are two ways to manufacture the lens with infill structure. Each layer of different infill structures can be constructed separately and then assembled into the complete lens structure. The other one is to use the special 3-D slicing software such as open-source Ultimaker Cura to form a multilayer slicing model with different infill ratios of each layer, as shown in Fig. 4. Then, the slicing model can be fabricated at a time by FDM 3-D printer.

It should be noted that considering the axial symmetry of relative permittivity distribution of Mikaelian lens, Table I only lists the air-hole sizes and infill ratios from layer No. 1 to layer No. 5.

B. Imaging Resolution and Surface Focusing Analysis

The NA of a lens is the most important design criteria in defining the imaging resolution characteristics for the focusing system, which depends on the refractive index of surrounding medium and the sine of the maximum ray angle. There are several definitions of the resolution criteria such as Rayleigh resolution limit of $0.61\lambda/\text{NA}$ and Abbe diffraction limit of $0.5\lambda/\text{NA}$ (λ is the wavelength). However, a more practical criterion that is adopted instead of the Abbe and Rayleigh criterion is the full-width at half-maximum (FWHM) of focal spot intensity, which is defined as follows [21]:

$$\text{FWHM} = 0.51\lambda/\text{NA}. \tag{4}$$

Obviously, higher values of NA mean that the better spatial resolution can be obtained with lens. The general form of NA of Mikaelian lens can be derived from the ray equation in the gradient index medium and determined using the following expression [22]:

$$\text{NA} = \sin\theta_m = \sqrt{n^2(x_0) - n^2(r)} \tag{5}$$

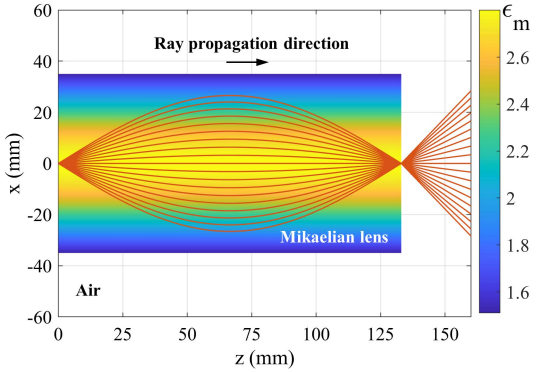

Fig. 5. Ray-tracing analysis of the proposed Mikaelian lens design for X-band based on the 2 × 2 ray transfer matrix (ABCD) theory.

where θ_m is the maximum cone angle at which a ray can be accepted by the aperture of lens, x_0 are the initial position of the ray in the aperture of lens, and r is the radius of lens.

Then, the FWHM of focal spot at the rear surface of lens

$$\mathrm{ML_{FWHM}} = \frac{0.51\lambda}{n_0\sqrt{1-\sec h^2(2\pi\, Pr/L)}}. \tag{6}$$

Here, for the designed lens operating at the X-band, $P = 0.5$, $L = 133$ mm, and $r = 35$ mm. Equation (6) then gives a maximum NA of 1.136, which corresponds to the theoretical imaging resolution limit of 0.45λ. Meanwhile, the theoretical maximum NA and FWHM for the designed lens operating at the Ka-band ($P = 0.5$, $L = 50$ mm, and $r = 13.5$ mm) are 1.155 and 0.44λ, respectively. Obviously, in both cases, the theoretical imaging resolution limit of designed lens is around 0.45λ.

To illustrate the focusing performance, a ray-tracing procedure (MATLAB source code provided in the Appendix) to verify the proposed lens design is performed based on the 2 × 2 ray transfer matrix (ABCD) theory [23]. Here, for the sake of brevity, the ray trajectory of the proposed lens design for the X-band is only shown in Fig. 5. As expected, the rays start from the center point of lens front surface and eventually intersect perfectly at a focal point on the rear surface of lens. The same ray-tracing procedure of lens design for the Ka-band can be performed to get the same results by using the abovementioned MATLAB code.

Moreover, the high-resolution focusing performances of the proposed cylindrical Mikaelian lens from 8.2 to 12.5 GHz are presented in Fig. 6. The WR-90 waveguide operating at the X-band with polarization along the y-axis is placed at the center point of lens as a feed source. By using the full-wave electromagnetic simulation using CST Microwave Studio, the 2-D electric field distribution at the yoz and xoy planes from 8.2 to 12.5 GHz inside lens is given in Fig. 6(a)–(c), respectively. Considering that the surrounding space of the simulation lens model is the free space, the open boundary condition with some extra space added between the structure and the applied boundary condition is applied along all the directions. After propagating through lens, the electromagnetic waves are well concentrated to a focusing spot on the rear surface of lens. Obviously, the results of these two methods are in reasonable agreement, which indicates that the proposed lens design at the

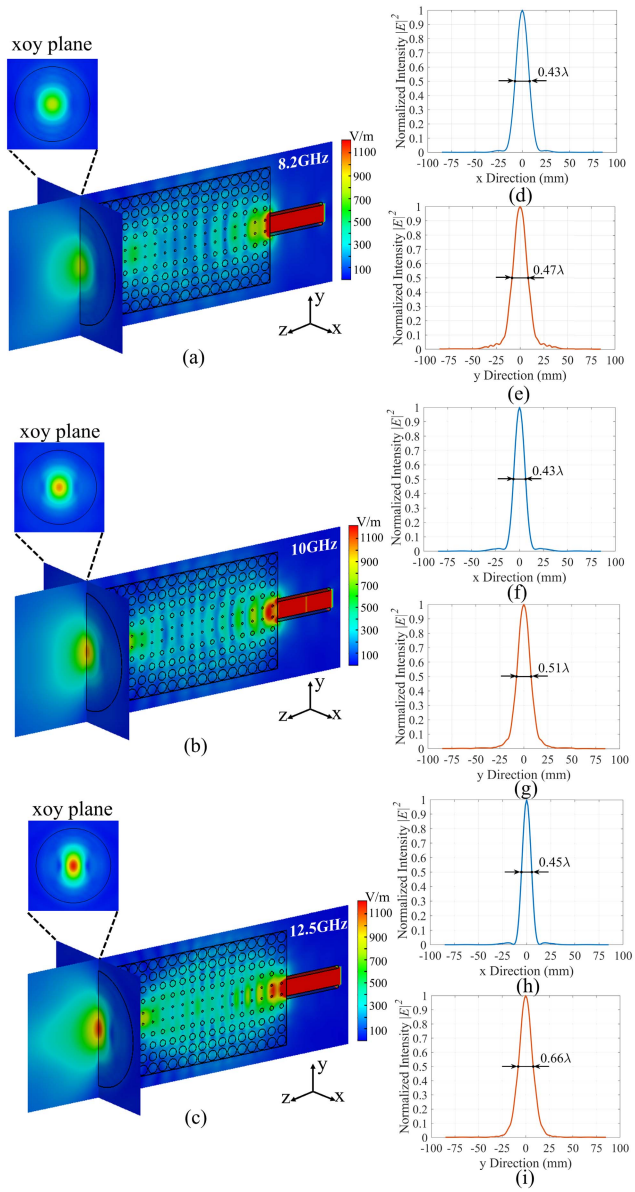

Fig. 6. High-resolution focusing performances of the proposed Mikaelian lens at the X-band. (a)–(c) Simulated 2-D electric field distribution at 8.2, 10, and 12.5 GHz, respectively, with waveguide operating at the X-band with polarization along the y-axis as source feed. (d)–(i) Normalized electric intensity $|E|^2$ profiles along the x- and y-directions at the focusing plane (xoy plane) at 8.2, 10, and 12.5 GHz.

X-band can be a good phase transformer to convert a diverging spherical wave into a converging spherical wave.

In order to quantitatively analyze the focusing performance of the proposed lens design, the normalized electric intensity $|E|^2$ profiles along the x- and y-directions at the focusing plane (xoy plane) from 8.2 to 12.5 GHz are shown in Fig. 6(d)–(i). The values of FWHM for the normalized electric intensity profile along the x-direction are all around 0.45λ. Although the values of FWHM for the electric intensity profile along the y-direction tend to increase as the frequency increases, the variation is not very large (less than 0.15λ) considering the open-ended waveguide as the feeding source.

Besides, the simulation model of Mikaelian lens operating at the Ka-band is composed of five concentric circular cylinders

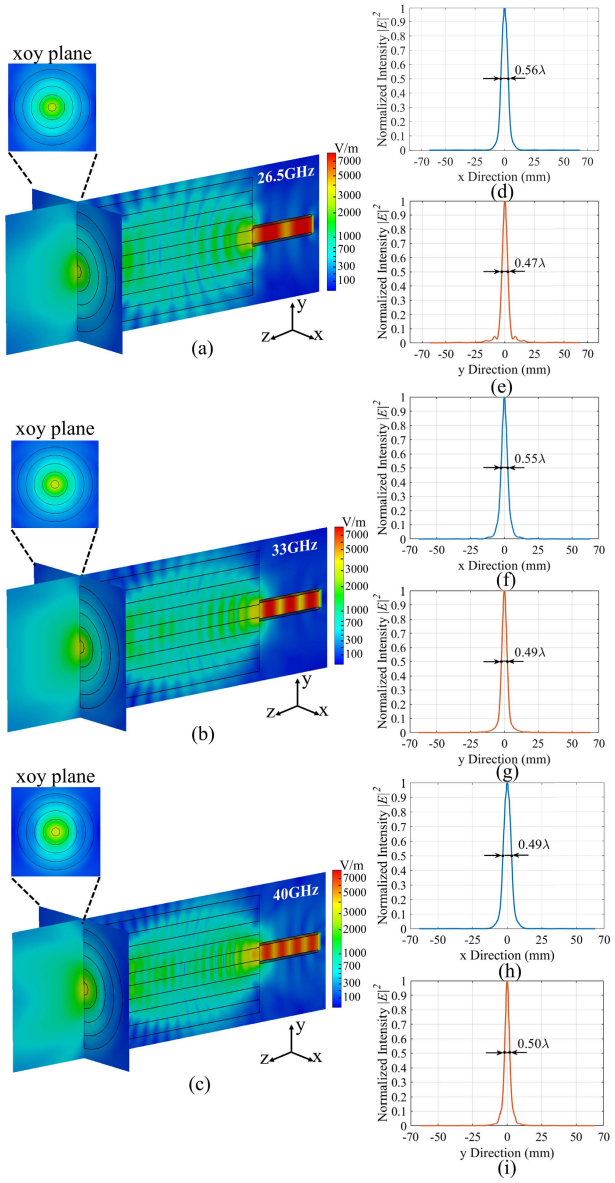

Fig. 7. High-resolution focusing performances of the proposed Mikaelian lens at the *Ka*-band. (a)–(c) Simulated 2-D electric field distribution at 26.5, 33, and 40 GHz, respectively, with waveguide operating at *Ka*-band with polarization along the *y*-axis as source feed. (d)–(i) Normalized electric intensity $|E|^2$ profiles along the *x*- and *y*-directions at the focusing plane (*xoy* plane) at 26.5, 33, and 40 GHz.

with radially varied permittivity of 1.665, 2.061, 2.423, 2.681, and 2.775. The same procedure is performed to obtain the simulated 2-D electric field distribution at the *yoz* plane from 26.5 to 40 GHz, as shown in Fig. 7(a)–(c). Similarly, the electromagnetic waves can also be concentrated to a focusing spot on the rear surface of lens, which further indicates that the proposed lens concept can be applied in higher frequency bands very well. As shown in Fig. 7(d)–(i), the values of FWHM for the normalized electric intensity profile along the *x*- and *y*-directions are all around 0.5λ. Due to the limited number of discrete concentric circular cylinders in the simulation model, the small differences between theoretical and simulated FWHM occur. Overall, the designed Mikaelian lens operating at these two frequency bands can achieve the subwavelength imaging resolution of 0.5λ.

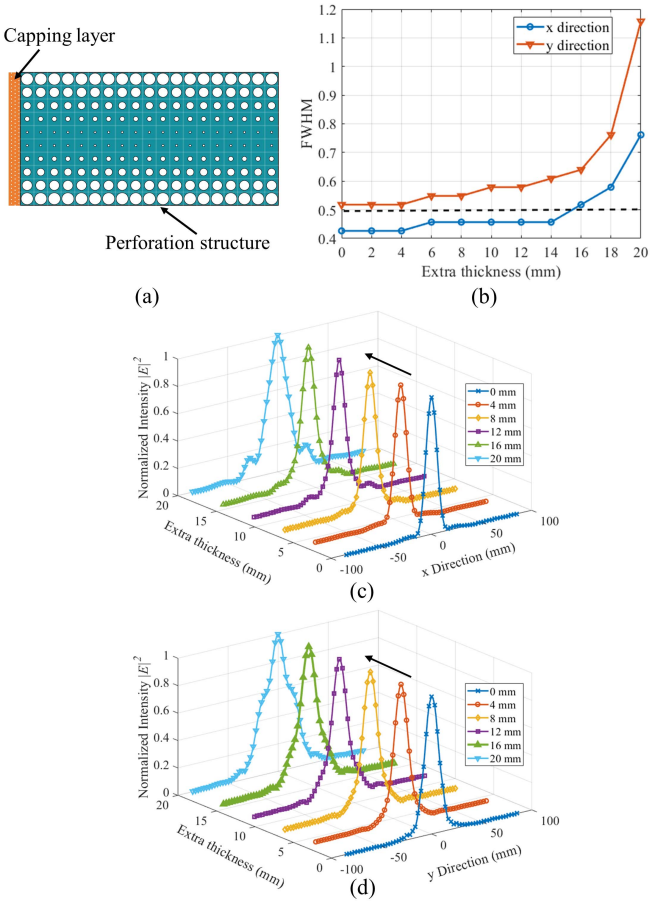

Fig. 8. (a) Schematic of a capping layer on the top of designed perforation structure. (b) Relationship between FWHM and the thickness of the capping layer along the *x*- and *y*-directions at the designed frequency of 10 GHz. (c) and (d) Normalized electric intensity $|E|^2$ profiles along the *x*- and *y*-directions with different thicknesses at 10 GHz.

C. Influence of Manufacturing Process on Perforation Structure

As mentioned above, the infill structure with different infill ratios can be automatically and accurately realized by the slicing software. Here, we only focus on the analysis of the influence of fabrication process on the imaging resolution of the lens with perforation structure. In the actual 3-D printing process, to ensure the stability of the perforation structure, a capping layer needs to be added on the top of designed perforation structure, as shown in Fig. 8(a). However, this operation increases the length of the lens, which further affects the imaging resolution according to (6). In order to better understand the effects of capping layer, parametric studies have been carried out by changing the thickness of capping layer in the simulation model. Fig. 8(c) and (d) shows the normalized electric intensity $|E|^2$ profiles along the *x*- and *y*-directions with different thicknesses at a designed frequency of 10 GHz. It is readily understood that the FWHM increases as the thickness of the capping layer increases. However, the change of FWHM along both the *x*- and *y*-directions is not obvious within the thickness range between 0 and 4 mm, as shown in Fig. 8(b). It demonstrates the practicability of using a thin capping layer to enhance the stability of perforation structure.

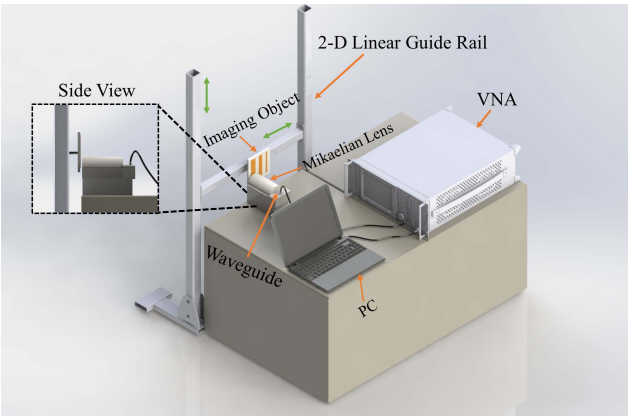

Fig. 9. 3-D perspective view of the proposed single-pixel scanning microwave/millimeter-wave imaging measurement setups.

III. Experimental Results and Discussion

A. Microwave/Millimeter-Wave Imaging Measurement Setups

Fig. 9 shows the schematic 3-D view of the proposed single-pixel scanning microwave/millimeter-wave imaging measurement setups. It consists of four main parts: the designed cylindrical Mikaelian lens, standard waveguide, vector network analyzers (VNAs), and 2-D linear guide rail. The scanning process and data collection are performed automatically by using the control application under the LabVIEW environment. The spatial resolution imaging experiment was performed by the time-domain measurement method [24], [25], [26] that is very common and mature. The corresponding fast Fourier transform (FFT)/inverse fast Fourier transform (IFFT) routines and Chirp-Z transforms are available in the VNA.

Here, the standard waveguide operating at the X- and Ka-band not only serves as a microwave transmitter (Tx) but also works as a receiver (Rx). The imaging object is fixed on the 2-D linear guide rail and is moved in the horizontal and vertical directions step by step. The measured echoed signals ($S11$ parameter) for each of the reflecting points (or pixels) at the imaging object can be recorded by VNA in the frequency domain. Then, the raw datasets of measured $S11$ can be automatically transformed into a time-domain signal using FFT/IFFT routines embedded code in the VNA, which forms a 2-D image. It should be noted that image processing algorithm, such as image denoising and imaging enhancement technique, is not used in our case to demonstrate the characteristic of sub-wavelength imaging resolution of the proposed Mikaelian lens.

Here, for the sake of brevity, Fig. 10 just shows the foam-based measurement setup for single-pixel scanning microwave imaging. In this case, the designed lens prototype operating at the X-band is utilized. While not blocking the movement of the 2-D linear guide rail, the actual distance between the imaging target and the lens is required to be kept as small as possible. Note that the measurement setup for millimeter-wave imaging by using a lens prototype operating at the Ka-band is similar to this one.

B. Spatial Resolution Performance of Designed Mikaelian Lens Operating at X-Band

The imaging object consists of plastic bottom plate and three copper sheets with different physical widths of 10, 15, and 20 mm, as shown in Fig. 11(a). The size of the entire scanning area is 102 × 102 mm. In our case, the distance of each movement for 2-D linear guide rail is set to 2 mm. In other words, the actual physical distance represented by one pixel is 2 mm. Considering the proposed Mikaelian lens operating at the design frequency of 10 GHz, the magnitude of the reflection coefficient at this frequency is used for the experimental characterization of the imaging resolution. Fig. 11(b) shows the measured normalized magnitude of the reflection coefficient for the imaging object at 10 GHz. Because of a very small focal spot with the theoretical FWHM of 0.45λ at the rear surface of lens, only a small area is illuminated at each measurement point. Thus, the three copper sheets can be clearly distinguished. Moreover, the measured width of three copper sheets is about 7, 8, and 10 pixels, as shown in Fig. 11(b). It means that a spatial resolution of 0.5λ (15 mm) is achievable with this measurement setup.

The complete set of measured normalized magnitude of the reflection coefficient at 8.5, 9, 10, 11, 12, and 12.5 GHz is presented in Fig. 12. It can be observed that three copper sheets can be still clearly distinguished, which further demonstrates the certain broadband behavior of the designed lens prototype. Due to the small distance between copper sheets and the effect of plastic bottom plate, the unwanted noise signal can be clearly seen around the imaging object, which causes the slight quality degradation in imaging.

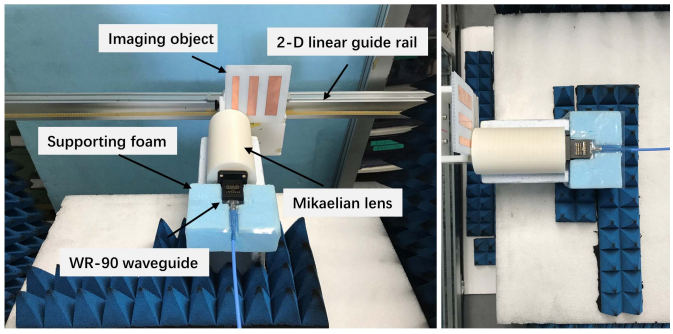

Fig. 10. Photograph of single-pixel scanning microwave imaging measurement setup by using the Mikaelian lens prototype operating at the X-band.

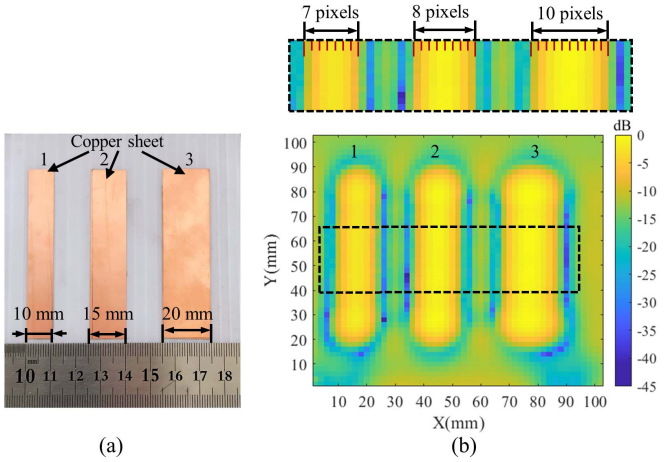

Fig. 11. (a) Imaging object with different widths (10, 15, and 20 mm) of copper sheets and plastic bottom plate. (b) Measured normalized magnitude of the reflection coefficient for three copper sheets at 10 GHz with a width of 7, 8, and 10 pixels (from left to right). Note that the actual physical distance represented by 1 pixel is 2 mm in this case.

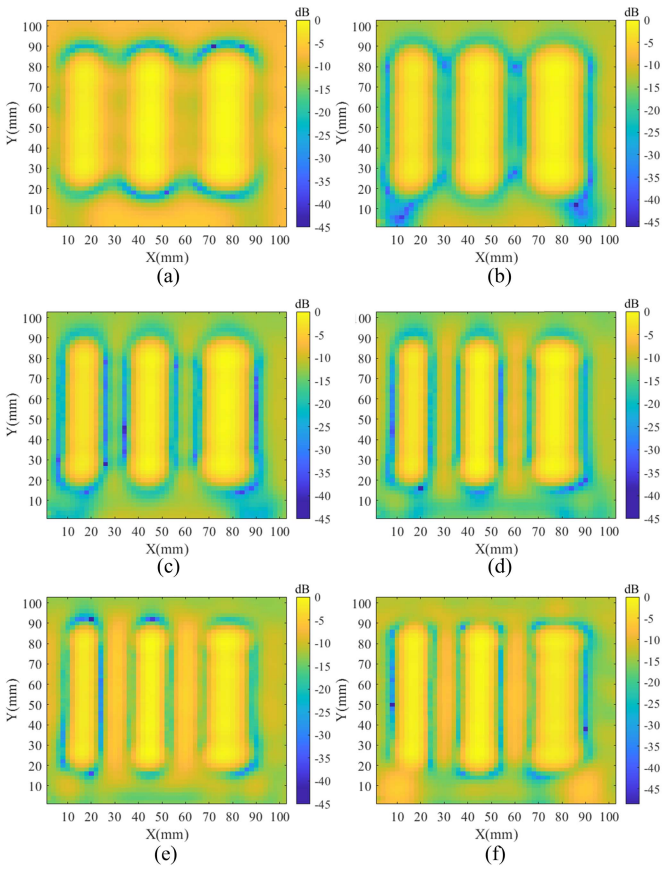

Fig. 12. Measured normalized magnitude of the reflection coefficient for three copper sheets at (a) 8.5, (b) 9, (c) 10, (d) 11, (e) 12, and (f) 12.5 GHz.

C. Spatial Resolution Performance of Designed Mikaelian Lens Operating at Ka-Band

As the size of the imaging target is further reduced, the effects of unwanted noise caused by the small distance between copper sheets and plastic bottom plate on the imaging cannot be ignored. In order to eliminate its interference on high-frequency imaging as much as possible, foam absorber material is utilized instead of plastic bottom plate in the spatial resolution imaging experiment at the *Ka*-band. Fig. 13(a) shows the photograph of imaging object with two copper sheets with different physical widths of 5 and 10 mm. Here, the size of the entire scanning area is 31 $\times$ 31 mm. The distance of each movement for 2-D linear guide rail is set to 1 mm. Similarly, after the electromagnetic waves pass through the designed lens at the *Ka*-band, it can also be concentrated to a subwavelength focusing spot on the imaging object. As shown in Fig. 13(b), the two copper sheets with measured width of 6 and 11 pixels are clearly distinguished at the design frequency of 30 GHz, which indicates that the spatial resolution of 0.5λ (6 mm) for designed lens prototype can also be achieved.

In addition, due to the existence of foam absorber material, the interference of unwanted noise signal between two copper sheets is effectively eliminated. The complete set of measured magnitude of the reflection coefficient at 27, 30, 33, 36, 38, and 40 GHz is given in Fig. 14. Two copper sheets can be still clearly distinguished at these frequencies, which

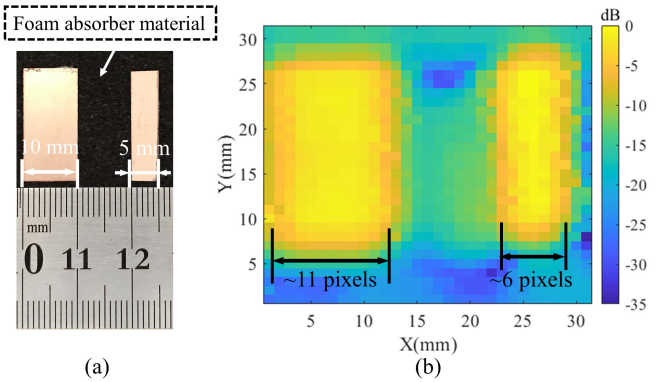

Fig. 13. (a) Imaging object with different widths (5 and 10 mm) of copper sheets. (b) Measured normalized magnitude of the reflection coefficient for two copper sheets at 30 GHz with a width of 6 and 11 pixels. Note that the actual physical distance represented by one pixel is 1 mm in this case.

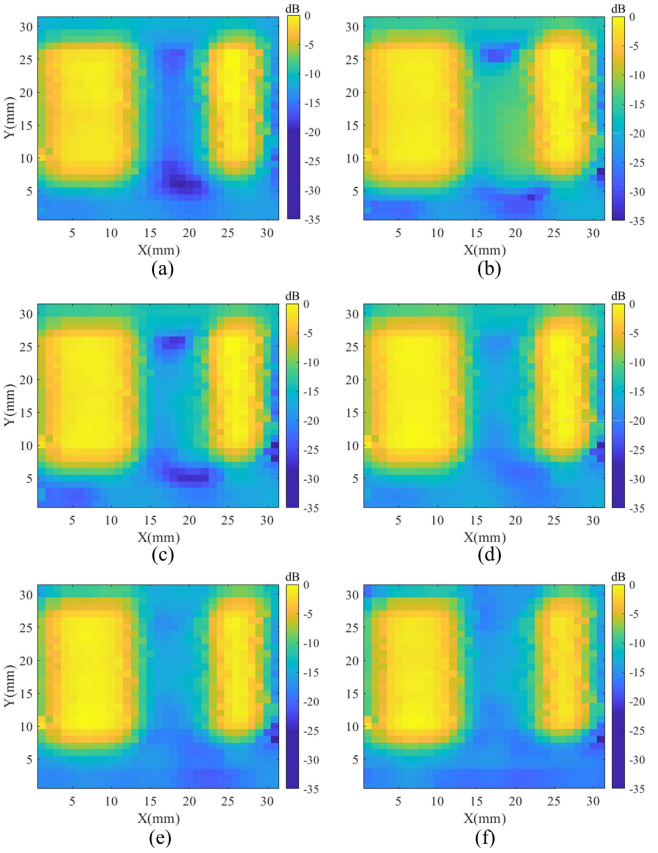

Fig. 14. Measured normalized magnitude of the reflection coefficient for three copper sheets at (a) 27, (b) 30, (c) 33, (d) 36, (e) 38, and (f) 40 GHz.

further demonstrates that the proposed lens concept can be applied in higher frequency bands very well. Most importantly, the broadband behavior of the proposed lens can also be maintained.

D. Target Imaging of Letters

To verify the effect of the object's shape and orientation on the imaging system, a Japanese romaji word "TOHOKU" engraved in two single-sided copper clad laminates is utilized, as shown in Fig. 15(a) and (b). The linewidth of each letter of the word "TOHOKU" is slightly less than 15 mm. Here, the

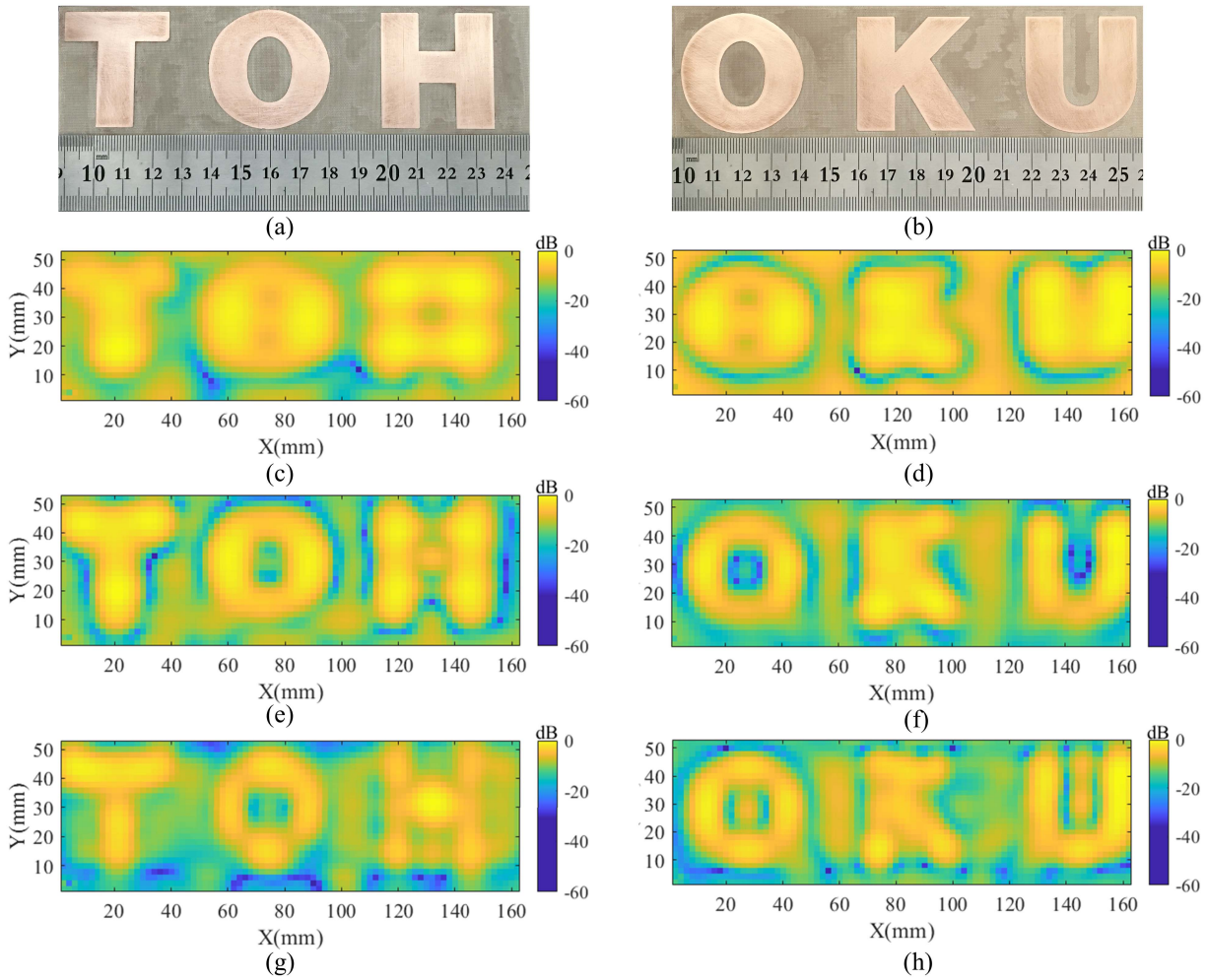

Fig. 15. (a) and (b) Japanese romaji word "TOHOKU" engraved in two single-sided copper clad laminate. (c)–(h) Measured normalized magnitude of the reflection coefficient for the word "TOHOKU" at 8.5, 10, and 12.5 GHz by using a designed lens prototype operating at the X-band. Note that the actual physical distance represented by 1 pixel is 2 mm in this case.

TABLE II

PERFORMANCE COMPARISON BETWEEN THE PROPOSED AND THE REPORTED LENS

References	Frequency [GHz]	Aperture diameter or size [λ]	Imaging distance [λ]	FWHM	Imaging resolution [λ]	Lens material	Lens style
This work	10, 30	2.3, 2.7	0	~0.5λ	0.5, ~0.6	PLA	cylindrical lens
[27]	16.4	1.4 × 7.7	0.6	0.55λ	0.55	HiK 500F	Photonic-crystal flat lens
[28]	108	~6.5	4.3	-	~0.9	MACO	catadioptric lens
[29]	652	108.7	54.3	-	3.1	PTFE	aspheric lens
[2]	77	128.5	771.2	-	5.1	PE	aspheric lens
[30]	70~110	107.5~168.5	584.1~915.7	-	4.7~7.3	-	aspheric lens
[31]	94	109.7	783.7	-	2.1	PE	aspheric lens

measured magnitude of the reflection coefficient for the word "TOHOKU" at 8.5, 10, and 12.5 GHz is measured by using a designed lens prototype operating at the X-band, as shown in Fig. 15(c)–(h). Although the scanning image of "TOHOKU" can be recognized, it suffers from some degree of distortion. This is mainly attributed to the limited spatial resolution of 0.5λ (15 mm) for the lens prototype operating at the X-band. In particular, it is different to identify the letters with complex shapes such as "H" and "K." In addition, because of the single-polarization standard waveguide as the microwave receiver, the orientation information of each letter cannot be recorded, which further increases image distortion. However, this phenomenon provides the possibility to enhance the image quality by using multipolarization information when the size of imaging target is comparable to the spatial resolution.

Fig. 16 shows the measured magnitude of the reflection coefficient for the word "TOHOKU" at 27, 33, and 40 GHz by using a designed lens prototype operating at the *Ka*-band. As mentioned in Section III-C, the spatial resolution of 0.5λ (6 mm) for designed lens prototype at the design frequency of 30 GHz can be achieved, which is much smaller than the linewidth of 15 mm for each letter of the word "TOHOKU."

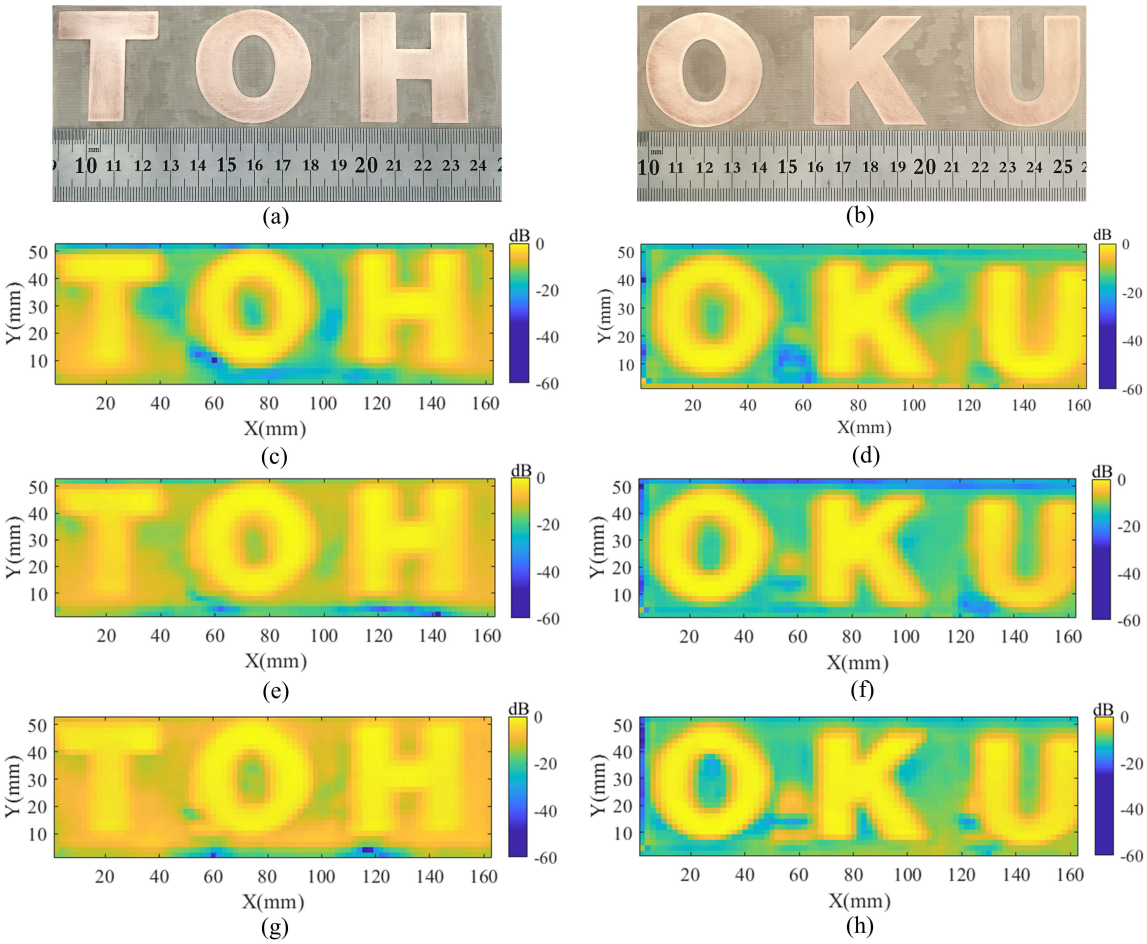

Fig. 16. (a) and (b) Japanese romaji word "TOHOKU" engraved in two single-sided copper clad laminate. (c)–(h) Measured normalized magnitude of the reflection coefficient for the word "TOHOKU" at 27, 33, and 40 GHz by using a designed lens prototype operating at the *Ka*-band. Note that the actual physical distance represented by 1 pixel is 2 mm in this case.

Obviously, as shown in Fig. 16(c)–(h), each letter of the word "TOHOKU" can be recognized perfectly in the scanning image. Although the single-polarization standard waveguide is also utilized as the receiver, the complex shape and different orientations of letters do not have negative effects on imaging quality in this case. It also proves that the smaller focusing spot size is key to achieve high-quality imaging. Overall, the proposed Mikaelian lens prototype exhibits excellent imaging performance with high resolution. The functionality of this lens concept can also be easily expanded to higher frequency bands.

Table II gives a brief comparison of the proposed cylindrical Mikaelian lens operating at the *X*- and *Ka*-band with other lens designs published in the literature. Here, it should be noted that the parameter of FWHM is not given directly in [24], [25], [26], [27], and [28].

IV. Conclusion

In this article, an all-dielectric surface focusing Mikaelian lens operating at the *X*- and *Ka*-band was proposed to achieve high-resolution focusing with theoretical FWHM around 0.45λ for the single-pixel scanning microwave and millimeter-wave imaging. The realization of the proposed Mikaelian lens employs the perforated structure with different air-hole sizes and infill structure with different infill ratios of PLA material by using easily accessible 3-D printing technology at a very low cost. Combining ray-tracing analysis and full-wave electromagnetic simulation, the surface focusing properties of subwavelength spot size for the designed lens has been validated at the *X*- and *Ka*-band, revealing the advantage of broad bandwidth. Moreover, based on the time-domain measurement method, the spatial resolution imaging experiment was carried out to demonstrate the excellent imaging performance for the designed lens prototype with a high resolution of 0.5λ, which reveals great potential for high-resolution microwave and millimeter-wave imaging applications. Besides, the functionality of the proposed lens concept can be further expanded to higher frequency bands such as THz by using advanced nanotechnology.

Appendix

The MATLAB source code of ray-tracing procedure in Section II-B is available at the following link. https://drive.google.com/file/d/17FB76_Ss4PLxl-pmbNzcnixlpVKNM42q/view?usp=sharing.

Acknowledgment

The author sincerely thanks Dr. X. T. Li from Tohoku University for helpful discussions about experimental measurement.

REFERENCES

[1] R. Appleby and H. B. Wallace, "Standoff detection of weapons and contraband in the 100 GHz to 1 THz region," *IEEE Trans. Antennas Propag.*, vol. 55, no. 11, pp. 2944–2956, Nov. 2007.

[2] H. Sato *et al.*, "Development of 77 GHz millimeter wave passive imaging camera," in *Proc. IEEE Sensors*, Oct. 2009, pp. 1632–1635.

[3] Y. Cheng, Y. Wang, Y. Niu, H. Rutt, and Z. Zhao, "Physically based object contour edge display using adjustable linear polarization ratio for passive millimeter-wave security imaging," *IEEE Trans. Geosci. Remote Sens.*, vol. 59, no. 4, pp. 3177–3191, Apr. 2021.

[4] S. Kharkovsky, J. T. Case, M. A. Abou-Khousa, R. Zoughi, and F. L. Hepburn, "Millimeter-wave detection of localized anomalies in the space shuttle external fuel tank insulating foam," *IEEE Trans. Instrum. Meas.*, vol. 55, no. 4, pp. 1250–1257, Aug. 2006.

[5] S. Ahdi Rezaeieh, A. Darvazehban, M. Khosravi-Farsani, and A. M. Abbosh, "Body-matched gradient index lens antenna for electromagnetic torso scanner," *IEEE Trans. Antennas Propag.*, vol. 69, no. 10, pp. 6165–6174, Oct. 2021.

[6] W. C. Choi, S. Lim, and Y. J. Yoon, "Design of noninvasive hyperthermia system using transmit-array lens antenna configuration," *IEEE Antennas Wireless Propag. Lett.*, vol. 15, pp. 857–860, 2016.

[7] A. Omar, "Baseband and super-resolution-passband reconstructions in microwave imaging," *IEEE Trans. Microw. Theory Techn.*, vol. 67, no. 4, pp. 1327–1335, Apr. 2019.

[8] W. Fan, B. Yan, Z. Wang, and L. Wu, "Three-dimensional all-dielectric metamaterial solid immersion lens for subwavelength imaging at visible frequencies," *Sci. Adv.*, vol. 2, no. 8, Aug. 2016, Art. no. e1600901.

[9] E. T. F. Rogers *et al.*, "A super-oscillatory lens optical microscope for subwavelength imaging," *Nature Mater.*, vol. 11, pp. 432–435, Mar. 2012.

[10] N. Yu *et al.*, "Light propagation with phase discontinuities: Generalized laws of reflection and refraction," *Science*, vol. 334, no. 6054, pp. 333–337, Oct. 2011.

[11] V. V. Kotlyar, A. A. Kovalev, and A. G. Nalimov, "Planar gradient hyperbolic secant lens for subwavelength focusing and superresolution imaging," *Optics*, vol. 1, no. 1, pp. 1–10, Dec. 2012.

[12] A. G. Nalimov and V. V. Kotlyar, "Hyperbolic secant slit lens for subwavelength focusing of light," *Opt. Lett.*, vol. 38, no. 15, pp. 2702–2704, Aug. 2013.

[13] S. S. Stafeev, E. S. Kozlova, A. G. Nalimov, and V. V. Kotlyar, "Tight focusing of a cylindrical vector beam by a hyperbolic secant gradient index lens," *Opt. Lett.*, vol. 45, no. 7, pp. 1687–1690, Mar. 2020.

[14] T. Baghdasaryan, T. Geernaert, H. Thienpont, and F. Berghmans, "Photonic crystal Mikaelian lenses and their potential use as transverse focusing elements in microstructured fibers," *IEEE Photon. J.*, vol. 5, no. 4, Aug. 2013, Art. no. 7100512.

[15] W. Shao and Q. Chen, "2-D beam-steerable generalized Mikaelian lens with unique flat-shape characteristic," *IEEE Antennas Wireless Propag. Lett.*, vol. 20, no. 10, pp. 2033–2037, Oct. 2021.

[16] F. Maggiorelli, A. Paraskevopoulos, J. C. Vardaxoglou, M. Albani, and S. Maci, "Profile inversion and closed form formulation of compact GRIN lenses," *IEEE Open J. Antennas Propag.*, vol. 2, pp. 315–325, 2021.

[17] J. Chen *et al.*, "Conformally mapped Mikaelian lens for broadband achromatic high resolution focusing," *Laser Photon. Rev.*, vol. 15, no. 5, Mar. 2021, Art. no. 2000564.

[18] A. L. Mikaelian, "Self-focusing medium with variable index of refraction," *Prog. Opt.*, vol. 31, pp. 283–346, Jan. 1980.

[19] T. Hayat, M. U. Afzal, A. Lalbakhsh, and K. P. Esselle, "Additively manufactured perforated superstrate to improve directive radiation characteristics of electromagnetic source," *IEEE Access*, vol. 7, pp. 153445–153452, 2019.

[20] S. Zhang, R. K. Arya, S. Pandey, Y. Vardaxoglou, W. Whittow, and R. Mittraj, "3D-printed planar graded index lenses," *IET Microw., Antennas Propag.*, vol. 10, no. 13, pp. 1411–1419, 2016.

[21] G. Kulaitis, "A statistical model of microscope resolution," Ph.D. dissertation, Inst. Math. Stochastics, Univ. Göttingen, Göttingen, Germany, 2020.

[22] D. W. Hewak and J. W. Y. Lit, "Solution deposited optical waveguide lens," *Appl. Opt.*, vol. 28, no. 19, pp. 4190–4198, Oct. 1989.

[23] W. Y. Shao, H. Sato, X. T. Li, K. K. Mutai, and Q. Chen, "Perforated extensible 3-D hyperbolic secant lens antenna for directive antenna applications using additive manufacturing," *Opt. Exp.*, vol. 29, no. 12, pp. 18932–18949, Jun. 2021.

[24] Z. Briqech and A.-R. Sebak, "Millimeter-wave imaging system using a 60 GHz dual-polarized AFTSA-SC probe," in *Proc. 33rd Nat. Radio Sci. Conf. (NRSC)*, Feb. 2016, pp. 325–332.

[25] M. S. Saadat, S. Sur, S. Nelakuditi, and P. Ramanathan, "Millicam: Hand-held millimeter-wave imaging," in *Proc. 29th Int. Conf. Comput. Commun. Netw. (ICCCN)*, Aug. 2020, pp. 1–9.

[26] M. Perotoni, C. Junior, and K. Santos, "Conversion of scattering parameters to time-domain for imaging applications: Rules and examples," *J. Commun. Inf. Syst.*, vol. 36, no. 1, pp. 9–62, Mar. 2021.

[27] Z. Lu, J. A. Murakowski, C. A. Schuetz, S. Shi, G. J. Schneider, and D. W. Prather, "Three-dimensional subwavelength imaging by a photonic-crystal flat lens using negative refraction at microwave frequencies," *Phys. Rev. Lett.*, vol. 95, no. 15, Oct. 2005, Art. no. 153901.

[28] B. Banik, J. Vukusic, and J. Stake, "Millimeter wave characterization of a catadioptric lens for imaging applications," *IEEE Microw. Wireless Compon. Lett.*, vol. 19, no. 11, pp. 680–682, Nov. 2009.

[29] R. Zatta, R. Jain, J. Grzyb, and U. R. Pfeiffer, "Resolution limits of hyper-hemispherical silicon lens-integrated THz cameras employing geometrical multiframe super-resolution imaging," *IEEE Trans. THz Sci. Technol.*, vol. 11, no. 3, pp. 277–286, May 2021.

[30] Y. Cheng, L. Qiao, D. Zhu, Y. Wang, and Z. Zhao, "Passive polarimetric imaging of millimeter and terahertz waves for personnel security screening," *Opt. Lett.*, vol. 46, no. 6, pp. 1233–1236, Feb. 2021.

[31] W. G. Kim, N. W. Moon, M. K. Singh, H. K. Kim, and Y. H. Kim, "Characteristic analysis of aspheric quasi-optical lens antenna in millimeter-wave radiometer imaging system," *Appl. Opt.*, vol. 52, no. 6, pp. 1122–1131, Feb. 2013.

Wenyi Shao received the B.E. degree from Sichuan University, Chengdu, China, in 2013, and the M.E. degree from the University of Chinese Academy of Sciences, Beijing, China, in 2016. He is currently pursuing the Ph.D. degree at the Department of Communications Engineering, Tohoku University, Sendai, Japan.

His current research interests include lens antenna, low-profile gradient index (GRIN) lens, super-resolution microwave/millimeter-wave imaging technology, and passive millimeter-wave imaging systems.

Dr. Shao received the Japanese Government (Monbukagakusho: MEXT) Scholarship in 2017.

Qiang Chen (Senior Member, IEEE) received the B.E. degree from Xidian University, Xi'an, China, in 1986, and the M.E. and D.E. degrees from Tohoku University, Sendai, Japan, in 1991 and 1994, respectively.

He is currently a Chair Professor with the Electromagnetic Engineering Laboratory, Department of Communications Engineering, Faculty of Engineering, Tohoku University. His primary research interests include antennas, microwave and millimeter wave, electromagnetics measurement, and computational electromagnetics.

Dr. Chen is a Fellow of the Institute of Electronics, Information and Communication Engineers (IEICE). He received the Best Paper Award and Zen-Ichi Kiyasu Award in 2009 from the IEICE. He served as the Chair for the IEICE Technical Committee on Photonics-Applied Electromagnetic Measurement from 2012 to 2014, the IEICE Technical Committee on Wireless Power Transfer from 2016 to 2018, and the IEEE Antennas and Propagation Society Tokyo Chapter from 2017 to 2018. He is also the Chair of the IEICE Technical Committee on Antennas and Propagation.